Conceptual Approach for Precise Relative Positioning with Miniaturized GPS Loggers and Experimental Results

J. Traugott, F. Holzapfel and G. Sachs
Institute of Flight System Dynamics
Technische Universität München
GERMANY

johannes.traugott@tum.de

ABSTRACT

L1 phase measurements collected by a miniaturized and low cost GPS logging device are the basis for a navigation approach aiming to precisely measure (flight) trajectories independently from any auxiliary system. Forming single differences between two measurements taken by one moving receiver at two different times allows achieving relative precision in the low decimeter range over time intervals of up to several minutes. Neither space nor ground based augmentation systems, a second, nearby base receiver or any (static) initialization patterns are required by the method. This fact significantly reduces the complexity to be handled by the user often operating under adverse field conditions even at extremely remote locations. The approach is taking advantage of canceling ambiguities instead of striving for estimating these unknown quantities every phase measurement is biased with. The constitutive navigation equations are derived and theoretic aspects of various error sources restricting possible processing intervals are discussed in this paper. The method is validated by both static and dynamic reference data. Finally first results from a GPS campaign at Kerguelen Archipelago to measure the dynamic soaring of Albatrosses using the time-difference method are presented and exemplary data are processed using the time-difference method.

1.0 INTRODUCTION

The context the present navigation approach is developed in is a rather unconventional task: Exploring the question how (Wandering) Albatrosses, the world's largest birds, can fly thousands of miles over open seas without flapping their wings [21]. Considering the absence of vertical thermal up winds as utilized by birds (or glider planes) soaring over solid land mass, this capability becomes even more fascinating. Extensive research has been conducted on the theoretical aspects of the birds' flight technique named "dynamic soaring" – a cyclic maneuver performed in the shear wind field right above the water surface [13]. The maneuver and the geometry of an individual cycle are illustrated in Figure 1. Measuring suchlike maneuvers is complicated by multiple circumstances. For flight mechanical analysis position fixes are required with a relative precision to the maneuver's starting point in the decimeter range. High dynamics require high sampling rates of at least 10 Hz. The sensor used must operate completely autonomously and has to be lightweight (< 100 g) and small (< 150 x 50 x 20 mm^3). The weight restriction entails low power consumption for a runtime of up to 50 – 70 hours just as budget limitations and the risk of not recovering the device imply the use of low cost sensors. The latter requirements are readily met by standard single frequency GPS receiver modules as used in car navigation systems or latest generation cell phones. However, sufficient precision cannot be provided and satellite or ground based augmentation systems cannot be addressed due to the extremely remote habitat of the Albatross, compare Figure 2. Some of the GPS L1 receiver modules output raw data, i.e. pseudorange, carrier phase, Doppler frequency and raw signal strength or SNR values, with up to 10 Hz. Logging these raw (phase) measurements for sufficiently precise postprocessing instead of sticking to the code based online navigation solution qualifies these modules as appropriate sensors for the described flight measurement task. Note that the online navigation solution is restricted to sampling rates well below the rate the raw measurements are provided with.

Conventional phase based processing techniques rely on the presence of data collected by a nearby (≤ 10 km) base station and (mostly static) initialization patterns of the roving receiver. Both cannot be provided in the scope of the current applications: birds neither remain static nor close to a base station and can perform maneuvers inevitably causing signal shadowing resulting in complete loss of lock undoing any kind of initialization. Hence an alternative way to process the L1 phase measurements with no need for a base station or initialization patterns is discussed in this paper. The price to be paid for these advantages is a limitation in processing time to a view minutes. A detailed description of the theoretic concept is given as well as a practical validation by static experiments and flight tests with an experimental aircraft. Finally results from our Winter 2008/09 Albatross measurement campaign to Kerguelen Archipelago are presented.

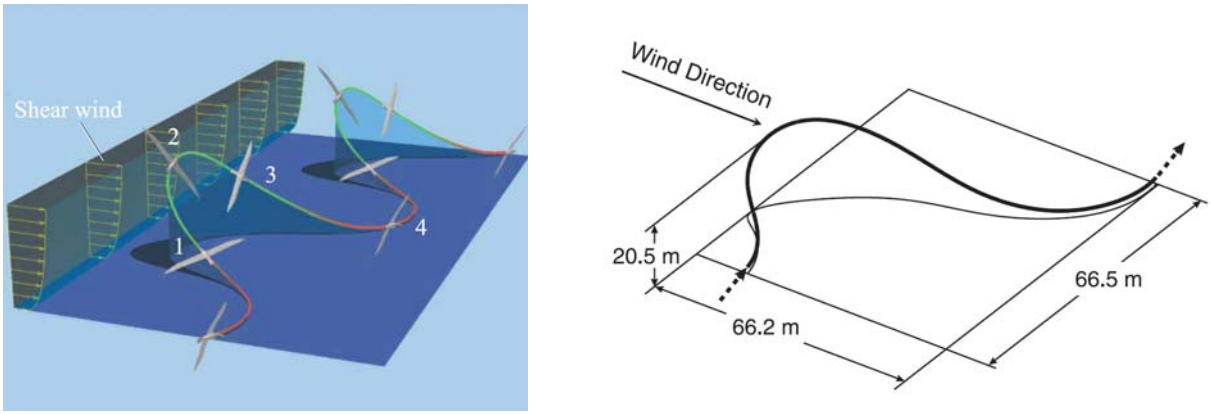

(a) Flight over water surface

(b) Geometry of a cycle, flown within approx. 7 – 10 sec

Figure 1: Dynamic soaring of Albatrosses [13]

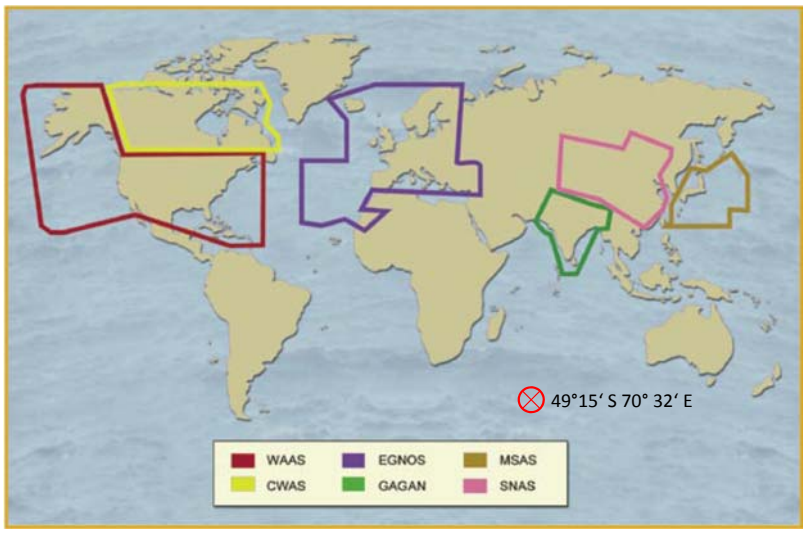

Figure 2: The habitat of the Wandering Albatross, Kerguelen Islands (red circle), with SBAS availabilitiy [6]

2.0 THEORETICAL BACKGROUND

2.1 The Observable: L1 Phase Ranges

The present method is based on the L1 phase range observable generated in the phase lock loop (PLL) of a GPS receiver. The nominal (constant) frequency f of the L1 carrier wave is 1575.42 MHz. Let $\varphi^S(t)$ [cycles] designate the phase of the satellite emitted wave as perceived by the receiver and $\varphi^R(t)$ [cycles] denote the phase of the (not yet Doppler compensated) receiver replica signal. With t [s] as an epoch in GPS system time reckoned from an initial epoch t_0 (= 0) when acquiring lock to the respective PRN one can state:

$$\varphi^S(t) = ft - f\frac{\rho(t)}{c} - \varphi_0^S(t) \qquad \varphi_0^S(t) = -\delta^S(t)f + \varphi^S(t_0) \tag{1}$$

$$\varphi^R(t) = ft - \varphi_0^R(t) \qquad \varphi_0^R(t) = -\delta^R(t)f + \varphi^R(t_0) \tag{2}$$

Here, φ_0^S and φ_0^R are the satellite and receiver initial phase biases at t_0 afflicted with the respective clock errors δ^S and δ^R [s] ($\delta > 0 \leftrightarrow$ clock reading ahead of GPS system time). The symbol ρ [m] is the geometric distance between satellite and receiver; c [m/s] denotes the nominal signal propagation speed in vacuum. The beat phase ϕ^{RS} [cycles] is now given by

$$\phi^{RS}(t) = \varphi^S(t) - \varphi^R(t) = -f\frac{\rho(t)}{c} - f\left(\delta^R(t) - \delta^S(t)\right) + \varphi^R(t_0) - \varphi^S(t_0) \tag{3}$$

Note that due to the initial distance between satellite and receiver $\rho(t_0)$, Eq. (3) theoretically yields a large decimal number for the beat phase $\phi^{RS}(t)$. However when acquiring lock to the respective PRN only the fractional part of this number can be measured, the initial integer number N of cycles between satellite and receiver is unknown. Note that this ambiguity is not time dependent as long as the phase is locked continuously: $N \neq N(t)$. Hence, to model the numerical value actually output by the receiver, this unknown but constant integer term N has to be subtracted from the right-hand side of Eq. (3). Moreover, to obtain a value directly corresponding to a geometric range, the result is multiplied by $-\lambda_1$ (the L1 wavelength) yielding the (pseudo) phaserange Φ [m]:

$$\Phi(t) = \rho(t) + c\left(\delta^R(t) - \delta^S(t)\right) + \lambda_1\underbrace{\left(\varphi^S(t_0) - \varphi^R(t_0) + N\right)}_{N'} \tag{4}$$

Neither the initial satellite nor receiver phase $\varphi^S(t_0)$, $\varphi^R(t_0)$ are known. Hence the non-integer ambiguity term N' is introduced as shown in Eq. (4) to finally rewrite for the L1 phaserange:

$$\Phi(t) = \rho(t) + c\left(\delta^R(t) - \delta^S(t)\right) + \lambda_1 N' \tag{5}$$

In literature the non-integer ambiguity term N' is frequently replaced by the integer ambiguity N. This is not precise in a strict sense but the fractional receiver and satellite phase terms only drop out and a truly integer ambiguity term is obtained when forming double differences. However, the non-integer character of the non-differenced phase observations does play an important role for procedures such as precise point positioning [7]. Keep in mind that the phase observable changes in the same sense as the C/A code pseudorange (negative Doppler) but is significantly less noisy.

2.2 Basic Concept

The principal idea of the present approach is the fact that the ambiguity N' is time-invariant, provided lock of phase. Hence, differencing phase observations to the same satellite S across two epochs t_b and t_i allows for canceling N':

$$^{bi}D\Phi = \Phi_i - \Phi_b = {}^{bi}D\rho + c\,{}^{bi}D\delta^R + \lambda_1 \underbrace{{}^{bi}DN'}_{0} \tag{6}$$

with D denoting single temporal differences. The right hand side subscript i shall be a short equivalent for the time argument (t_i) during the following derivations. Note that the satellite clock error $D\delta^S$ is neglected in Eq. (6).

The shown way to cancel ambiguities is the background for a diversity of applications. In tightly coupled GPS/INS systems time differenced double differences (so called triple differences across two receivers, two satellites and two epochs) can support the dynamics estimation for attitude computation [5]. In a similar context, also carrier phases directly differenced between subsequent epochs can be used instead of the noisier delta-range (Doppler) measurements to improve velocity and attitude information without the need for a base station [20]. Triple differences can also be used for carrier phase cycle slip detection [10]. Further, precise baseline computation between a base and a roving receiver provided that there are at least 7 satellites (if only phase data are used) in view is possible with triple differences [8]. Time-differences used in a stand-alone GPS application are used to process static data for gun-laying applications [17]. This approach, enhanced by a loop misclosure procedure, can be applied to static measurements from civil receivers since selective availability has been switched off [1].

Using time differences for processing kinematic data is an unconventional approach emerged from the need for a high quality but low effort navigation solution. The navigation equations are derived in the following.

2.3 Navigation Equations

Assume the position $\mathbf{x}$ of the receiver to be known at a (base) epoch t_b. Then one can write for the base vector pointing from the position at the base epoch to the position at the epoch of interest t_i

$$\mathbf{b}^{bi} = \mathbf{x}_i - \mathbf{x}_b \tag{7}$$

Figure 3 illustrates the geometry of the problem.

Besides the position, the receiver clock error with respect to GPS system time has to be determined, yielding the combined position and time (PT) variable:

$$\boldsymbol{\xi} = \left[\mathbf{x}^T, c\delta^R\right]^T \tag{8}$$

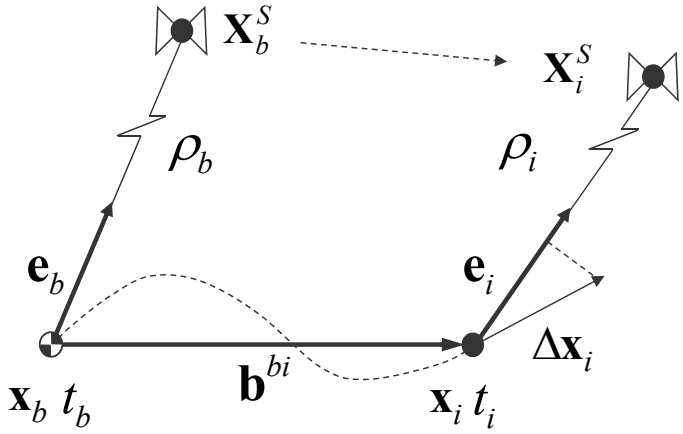

Figure 3: Basic principle of time differences

Here the clock error is scaled to range by multiplication with the signal propagation speed for convenience. Now one can set up the enhanced base vector:

$$\boldsymbol{\beta}^{bi} = \boldsymbol{\xi}_i - \boldsymbol{\xi}_b \tag{9}$$

In order to determine $\boldsymbol{\beta}^{bi}$, time differences ${}^{bi}D\Phi$ between two phase observations at t_b and t_i as introduced in Eq. (6) are used. For precise navigation, the phaserange, Eq. (5), has to be enhanced by models for signal delays caused by ionospheric and tropospheric refraction, $\hat{I}$ and $\hat{T}$:

$$\hat{\Phi}_i = \hat{\rho}_i + c\delta_i^R + \lambda_1 N' + \hat{T}_i - \hat{I}_i \tag{10}$$

Here the symbol ^ is introduced to distinguish modeled from measured values denoted ~ in the remainder. The geometric range is calculated by

$$\hat{\rho}_i = \left\| \mathbf{X}_i - \mathbf{x}_i \right\| \tag{11}$$

where $\mathbf{X}_i$ is the satellite position at the time of signal emission corresponding to the epoch t_i. This position (in conjunction with the respective emission time) is extracted from the Ephemeris data of the respective satellite. Now the time differenced phase observations can be rewritten as

$${}^{bi}D\hat{\Phi} = {}^{bi}D\hat{\rho} + c\,{}^{bi}D\delta^R - {}^{bi}D\hat{I} + {}^{bi}D\hat{T} = f\left(\xi_i, X_i, t_i, \xi_b, X_b, t_b\right) \tag{12}$$

with ξ_i as the only unknown. Note that in a strict sense $D\hat{\Phi}$ is not a function of $\boldsymbol{\beta}$ but of both the PT solution at the current epoch and the (known) base epoch. In order to solve for ξ_i, at least four measurements are required:

$${}^{bi}D\tilde{\boldsymbol{\Phi}} = {}^{bi}D\hat{\boldsymbol{\Phi}}\left(\boldsymbol{\xi}_i\right) \tag{13}$$

With

$${}^{bi}D\boldsymbol{\Phi} = \left[{}^{bi}D\Phi^1\ {}^{bi}D\Phi^2\ \ldots\ {}^{bi}D\Phi^m\right]^T; m \geq 4$$

Just as for standard single point processing, this (over-determined) set of equations is solved by the nonlinear least squares method. For that purpose, the right hand side of Eq. (13) has to be linearized:

$$ {}^{bi}D\hat{\mathbf{\Phi}}\left(\xi_i,\xi_b\right) = {}^{bi}D\hat{\mathbf{\Phi}}\left(\xi_{i,0},\xi_b\right) + \mathbf{H}_{\xi_{i,0}}\Delta\xi_i \tag{14} $$

The linearization point $\xi_{i,0}$ is either the result of the last iteration cycle of the current epoch or the final result of the previous epoch. The Jacobian writes elaborately as

$$ \mathbf{H}_{\xi_{i,0}} = \left.\frac{d\,{}^{bi}D\hat{\mathbf{\Phi}}}{d\xi_i}\right|_{\xi_{i,0}} = \left[\begin{array}{cccc} \frac{\partial\,{}^{bi}D\hat{\Phi}^1}{\partial x_i} & \frac{\partial\,{}^{bi}D\hat{\Phi}^1}{\partial y_i} & \frac{\partial\,{}^{bi}D\hat{\Phi}^1}{\partial z_i} & \frac{\partial\,{}^{bi}D\hat{\Phi}^1}{\partial\left(c\delta_i^R\right)} \\ \frac{\partial\,{}^{bi}D\hat{\Phi}^2}{\partial x_i} & \frac{\partial\,{}^{bi}D\hat{\Phi}^2}{\partial y_i} & \frac{\partial\,{}^{bi}D\hat{\Phi}^2}{\partial z_i} & \frac{\partial\,{}^{bi}D\hat{\Phi}^2}{\partial\left(c\delta_i^R\right)} \\ \vdots & \vdots & \vdots & \vdots \\ \frac{\partial\,{}^{bi}D\hat{\Phi}^m}{\partial x_i} & \frac{\partial\,{}^{bi}D\hat{\Phi}^m}{\partial y_i} & \frac{\partial\,{}^{bi}D\hat{\Phi}^m}{\partial z_i} & \frac{\partial\,{}^{bi}D\hat{\Phi}^m}{\partial\left(c\delta_i^R\right)} \end{array}\right]_{\xi_{i,0}} \tag{15} $$

With Eqs. (10) and (12) the following relationships hold

$$ \frac{\partial\,{}^{bi}D\hat{\Phi}}{\partial\mathbf{x}_i} \approx \frac{\partial\hat{\rho}_i}{\partial\mathbf{x}_i} = -\mathbf{e}_i; \quad \frac{\partial\,{}^{bi}D\hat{\Phi}}{\partial\left(c\delta_i^R\right)} = 1 \tag{16} $$

where $\mathbf{e}_i$ is the unit vector pointing from the rover position at t_i to the satellite, compare Figure 3. Spatial variations of the atmospheric models are neglected when linearizing as these effects are compensated for by the iteration. With Eq. (16) the Jacobian rewrites to

$$ \mathbf{H}_{\xi_{i,0}} = \begin{bmatrix} -\mathbf{e}_{i,0}^{1\,T} & 1 \\ \vdots & \vdots \\ -\mathbf{e}_{i,0}^{m\,T} & 1 \end{bmatrix} \tag{17} $$

Now one obtains with least squares for $\Delta\xi_i$

$$ \Delta\xi_i = \left(\mathbf{H}_{\xi_{i,0}}^T\mathbf{H}_{\xi_{i,0}}\right)^{-1}\mathbf{H}_{\xi_{i,0}}^T\left({}^{bi}D\tilde{\mathbf{\Phi}} - {}^{bi}D\hat{\mathbf{\Phi}}\left(\xi_{i,0},\xi_b\right)\right) \tag{18} $$

and iteration

$$ \xi_{i,k+1} = \xi_{i,k} + \Delta\xi_i \tag{19} $$

finally yields ξ_i. Note that even so this solution directly drops out of the solution process, ξ_i is precise relative to ξ_b only and its absolute accuracy depends on the one of ξ_b itself. Consequently, $\boldsymbol{\beta}^{bi}$ is the intrinsic solution of the problem. This will become even more evident in Eq. (28).

The shown solving procedure minimizes the residuals f^j between measured and modeled observations in a least squares sense:

$$\sum_{j=1}^{m}\left(f^{j}\right)^{2}=\min \tag{20}$$

$$f^{j}={}^{bi}D\widetilde{\Phi}^{j}-{}^{bi}D\hat{\Phi}^{j} \tag{21}$$

If the inevitable experimental measurement errors are uncorrelated, have a mean of zero and a constant variance, the least squares estimate of $\Delta\boldsymbol{\xi}_i$ has the minimum variance of all estimates that are linear combinations of the observations. In this sense it is the optimal solution.

2.4 Error Analysis

As indicated in Eq. (10) the phase range model is enhanced by terms taking into account atmospheric signal propagation delays. However, these effects cannot be eliminated completely. The remaining effects ε compose, together with other contributions, the non-modeled range error χ:

$$\begin{aligned}\widetilde{\Phi}_i&=\hat{\Phi}_i+\chi_i\\ \chi_i&=-c\delta_i^S+E_i+\varepsilon_i+\text{noise}+\text{multipath}\end{aligned} \tag{22}$$

This error is made up by the scaled satellite clock bias δ^S, the satellite position offset due to uncertainties in the satellite ephemeris E, the described remaining atmospheric delays ε, measurement noise and multipath. When forming time differences this yields

$$\begin{aligned}{}^{bi}D\widetilde{\Phi}&={}^{bi}D\hat{\Phi}+{}^{bi}D\chi\\ {}^{bi}D\chi&=-c\,{}^{bi}D\delta^S+{}^{bi}DE+{}^{bi}D\varepsilon+{}^{bi}D\,\text{noise}+{}^{bi}D\,\text{multipath}\end{aligned} \tag{23}$$

Except for the noise ($\sigma_{\nabla\text{noise}}\approx\sqrt{2}\sigma_{\text{noise}}$) and multipath, the range error components are highly temporally correlated which allows the following "linearization":

$${}^{bi}D\chi=\left[-c\frac{d\delta^S}{dt}+\frac{dE}{dt}+\frac{\partial\varepsilon}{\partial t}\right]_{t_b}\left(t_i-t_b\right)+\left.\frac{\partial\varepsilon}{\partial\mathbf{x}^R}\right|_{t_b}\mathbf{b}^{bi}+{}^{bi}D\,\text{noise}+{}^{bi}D\,\text{multipath} \tag{24}$$

The atmospheric error stemming from spatial variations occurs in any kind of differential processing and remains small with short baseline length. As a matter of fact, the raise of the noise level cannot be avoided but is smaller by a factor of $1/\sqrt{2}$ than when working with double differences. However, the drift terms are the bottleneck problem for the time difference approach. In order to keep this effect small, precise correction data are utilized. These data not only decrease the absolute range error but also increase its temporal correlation. Usually only little attention is paid to this fact which is key for extending the precise processing time when working with time differences [15]. However, there is yet another error source affecting the relative precision of the solution - the bias in $\boldsymbol{\xi}_b$ from the true position and time. In order to analyze this effect, Eq. (14) is linearized in both $\boldsymbol{\xi}_{i,0}$ and the true base position and time $\boldsymbol{\xi}_{b,0}$:

$${}^{bi}D\hat{\boldsymbol{\Phi}}\left(\boldsymbol{\xi}_i,\boldsymbol{\xi}_b\right)={}^{bi}D\hat{\boldsymbol{\Phi}}\left(\boldsymbol{\xi}_{i,0},\boldsymbol{\xi}_{b,0}\right)+\mathbf{H}_{\boldsymbol{\xi}_{i,0}}\Delta\boldsymbol{\xi}_i-\mathbf{H}_{\boldsymbol{\xi}_{b,0}}\Delta\boldsymbol{\xi}_b \tag{25}$$

with the Jacobian $\mathbf{H}_{\boldsymbol{\xi}_{i,0}}$ according to Eq. (17) and $\Delta\boldsymbol{\xi}_b=\boldsymbol{\xi}_b-\boldsymbol{\xi}_{b,0}$. Referring to Eqs. (10), (12) and (17) one gets for the second Jacobian

$$\mathbf{H}_{\xi_{b,0}} = -\left.\frac{\partial^{bi}\nabla\hat{\mathbf{\Phi}}(\xi_i,\xi_b)}{\partial\xi_b}\right|_{\xi_{b,0}} = \begin{bmatrix} -\mathbf{e}_{b,0}^{1\ T} & 1 \\ \vdots & \vdots \\ -\mathbf{e}_{b,0}^{m\ T} & 1 \end{bmatrix} \tag{26}$$

The minus sign is used for convenience only in order to obtain analogy between $\mathbf{H}_{\xi_{i,0}}$ and $\mathbf{H}_{\xi_{b,0}}$. Figure 3 illustrates the geometry of the unit vectors. The matrices $\mathbf{H}_{\xi_{b,0}}$ and $\mathbf{H}_{\xi_{i,0}}$ are closely related which allows again to linearize:

$$\mathbf{H}_{\xi_{b,0}} = \mathbf{H}_{\xi_{i,0}} + \dot{\mathbf{H}}_{\xi_i}(t_b - t_i) = \mathbf{H}_{\xi_{i,0}} + \begin{bmatrix} -\dot{\mathbf{e}}_{i,0}^{1\ T} & 0 \\ \vdots & \vdots \\ -\dot{\mathbf{e}}_{i,0}^{m\ T} & 0 \end{bmatrix}(t_b - t_i) \tag{27}$$

Note that Eq. (27) only takes into account changes due to the time elapsed between base and rover epoch not due to the motion of the receiver. The former does have a significant impact on the unit vectors due to the motion of the satellites themselves whereas the latter is neglected due to the far distance between receiver and satellites. Inserting Eq. (27) in Eq. (25) yields

$$\begin{aligned} {}^{bi}\nabla\hat{\mathbf{\Phi}}(\xi_i,\xi_b) = {}&{}^{bi}\nabla\hat{\mathbf{\Phi}}(\xi_{i,0},\xi_{b,0}) + \\ &+ \mathbf{H}_{\xi_{i,0}}\underbrace{(\Delta\xi_i - \Delta\xi_b)}_{\Delta\boldsymbol{\beta}^{bi}} + \underbrace{\dot{\mathbf{H}}_{\xi_i}(t_i - t_b)\Delta\xi_b}_{{}^{bi}D\chi_{geo}} \end{aligned} \tag{28}$$

The last term of Eq. (28) is unknown and can, in analogy to $D\chi$, Eq. (23), be interpreted as a geometric range error caused by variable satellite geometry:

$$\begin{aligned} {}^{bi}D\chi_{\text{geo}}^{j} &= -\dot{\mathbf{e}}_i^{j\,T}\Delta\xi_b(t_i - t_b) \\ {}^{bi}D\boldsymbol{\chi}_{\text{geo}} &= \left[{}^{bi}D\chi_{\text{geo}}^{1}, \ldots, {}^{bi}D\chi_{\text{geo}}^{m}\right]^T \end{aligned} \tag{29}$$

Just as the non-modeled range error $D\chi$, the geometric range error causes an error in the relative navigation solution.

Figure 4 aims to illustrate this effect: If the position at t_b is afflicted by an offset $\delta\mathbf{x}_b$, the vector $\mathbf{b}^{bi}$ is first of all translated by $\delta\mathbf{x}_b$ as well. This translation causes a shift of $\mathbf{x}_i$ by $\delta\mathbf{x}_b$ which is no error as relative precision is yet maintained. However, just as every other range error, also $\nabla\boldsymbol{\chi}_{\text{geo}}$ causes a distortion of $\mathbf{b}^{bi}$ to $\mathbf{b}^{bi*}$, indicated by $\delta\mathbf{b}^{bi}$ in the figure. This does degrade relative precision. It is interesting to note that the variation of the satellite geometry over time has virtually no impact on the relative solution if the initial position and time ξ_b is known exactly, $\delta\xi_b = 0$, no matter how long time intervals are processed.

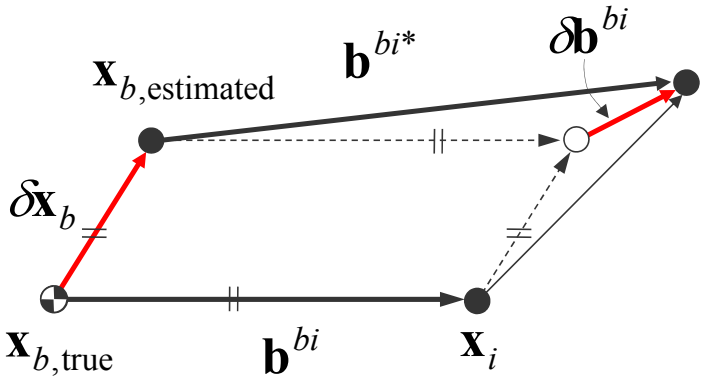

Figure 4: Impact of a bias in the initial epoch's position on relative precision

In order to estimate the impact of the various range errors on $\boldsymbol{\beta}^{bi}$, Eq. (23) is enhanced to

$$ {}^{bi}D\tilde{\Phi}^j = {}^{bi}D\hat{\Phi}^j + \underbrace{{}^{bi}D\chi^j + {}^{bi}D\chi^j_{\text{geo}}}_{{}^{bi}D\chi^j_{\text{total}}} \tag{30}$$

The total range error is a superposition of different random processes. Each of them has a different degree of temporal autocorrelation. For instance the change of the error caused by imprecise ephemeris is much slower than the change of the measurement noise. As only short time intervals $t_i - t_b$ are processed, the slowly changing error contributions can be considered as systematic but unknown biases in the measurements. In other terms, the individual range errors ${}^{bi}\nabla\chi^j_{\text{total}}$ can be assumed to be non-ergodic random processes with constant and equal variance and statistic distribution but a different, unknown expectation which is growing with time for each measurement. This fact significantly complicates the estimation of the error in $\boldsymbol{\beta}^{bi}$. In the scope of this paper, the quality of the solution is validated via comparison with reference solutions. In addition, a simplistic estimation of the error propagation is provided by referring to the concept of Dilution of Precision (DoP) as known from standard single point processing: Ignoring all systematic errors in the measurements for the lack of better knowledge, a rough estimation of the covariance matrix of the least squares solution is obtained by

$$\mathbf{C}_{\boldsymbol{\beta}} = \sigma^2_{\nabla\tilde{\Phi}}\mathbf{D}; \qquad \mathbf{D} = \left(\mathbf{H}^T_{\xi_{i,0}}\mathbf{H}_{\xi_{i,0}}\right)^{-1} \tag{31}$$

For the number of measurements exceeding the number of unknowns, $m \gg n = 4$, the variance of the measurements is estimated from the residuals by

$$\sigma^2_{D\tilde{\Phi}} \approx \frac{\sum_{j=1}^{m} f^{j^2}}{m-4} \tag{32}$$

Using the residuals from the solution between subsequent epochs, t_{n-1}, t_n, this represents the stochastic error component of the measurements. Using the residuals of the over-all solution, t_b, t_i, one obtains a quantity representing the error drift.

The DOP value referring to position accuracy is defined by

$$\text{PDOP} = \sqrt{\sum_{k=1}^{3} D_{kk}} \tag{33}$$

By comparing coefficients an estimate for either the 3D noise component or the 3D error drift is obtained by

$$\sqrt{\sum_{k=1}^{3} C_{\boldsymbol{\beta},kk}} = \sigma_{\nabla\tilde{\Phi}} \cdot \mathrm{PDOP} \tag{34}$$

Note that the Jacobian when working with time differences as indicated in Eq. (17) coincides with the one used when processing single points. Hence the numerical DOP values characterizing the quality of a single point solution also hold for the time difference solution.

3.0 IMPLEMENTATION

3.1 Two different implementation strategies

The above equations describe the core algorithm of the navigation task – the relative solution between two individual epochs. In order to implement a tool suitable for kinematic trajectory measurement, two different strategies can now be applied as shown in Figure 5.

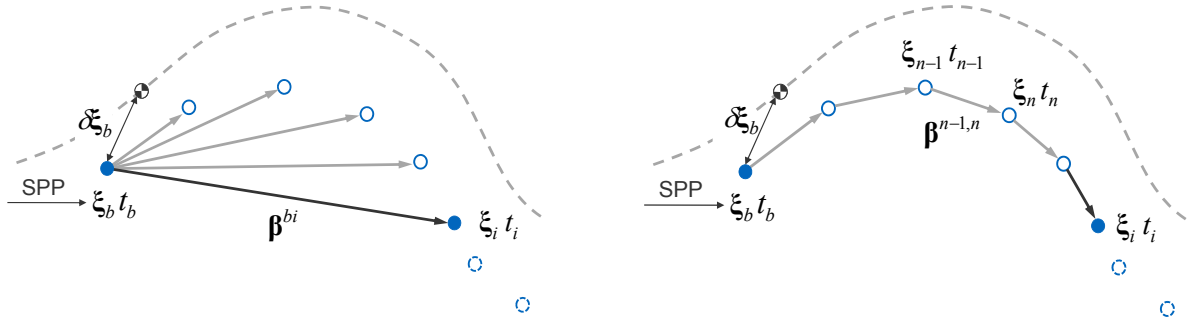

(a) Over-all solution **(b) Accumulated solution**

Figure 5: Different implementation strategies of the time-difference approach

In either case, the initial solution ξ_b is estimated by code-based single point processing (SPP) and therefore typically afflicted by an absolute error in the meter range ($\delta\xi_b$). The first strategy to obtain the complete trajectory is to calculate the "over-all solution" $\boldsymbol{\beta}^{bi}$ for each epoch as illustrated in Figure 5(a). Starting from the core-algorithm, this approach suggests itself – each epoch is calculated independently from all other observations and it is straightforward to judge the quality of the solution (error drift) via Eq. (34) based on the (raising) residual level $\sum \left({}^{bi}D\tilde{\Phi}^{j} - {}^{bi}D\hat{\Phi}^{j} \right)^2$, Eqs. (21) and (32). However, there are several caveats: The same subset of satellites must be available at both t_b and t_i. Considering that satellites might be lost on the way due to shadowing or antenna tilting, this is a severe restriction. Moreover signals which are once afflicted by cycle slips (r.t. the next section) must not be reused, unless there is a reliable repair algorithm. Another problem can occur with the drop-out of individual satellites which can induce small but sudden jumps in the trajectory – what may impede velocity determination via differentiation in the position domain. The alternative is to accumulate the position increments obtained by solving between subsequent epochs $\boldsymbol{\beta}^{n-1,n}$ as demonstrated by Figure 5(b). Accumulating error afflicted quantities always implies the risk of getting a random-walk like, unbound error. As demonstrated by various experiments and shown theoretically in [16], this is not the case here as the errors from the

incremental solution perfectly cancel when accumulating to the final solution. It turns out that the over-all and the accumulated solution are identical in a first order approximation given equivalent constellation geometry. Now the various advantages of the accumulation strategy become evident: The common subset of satellites between two subsequent epochs t_{n-1} and t_n can be used yielding generally improved geometries compared to the subset available at t_i and t_b (more common satellites available). Furthermore, cycle-slips do not propagate to subsequent epochs which makes a discrimination between simple outliers and cycle-slips obsolete when monitoring the integrity of the solution. However, estimating the error drift is based on the residual level of the over-all solution – a quantity which is no longer directly available but must be reconstructed by accumulating the residuals of the incremental solutions. This leads to overly pessimistic error drift estimates. Which strategy to chose depends on the data at hand and the respective application. If the data quality is good and error estimation is an important aspect, the over-all strategy is recommended. If the data quality is very poor, the accumulation strategy can be the only way to obtain a solution at all.

3.2 Receiver Autonomous Integrity Monitoring (RAIM)

If the signal tracking is subject to a temporary discontinuity, the integer part of the ambiguity N' may change while its fractional part remains constant – a so called cycle slip occurs. Such slip biases all subsequent observations of the respective channel. When using the over-all solution strategy, cycle slips are to be distinguished from other outliers and excluded for the present epoch and the future. When using the accumulation strategy, both outliers and cycle slips are to be excluded for the current epoch only but discrimination is obsolete. The detection and exclusion task is addressed by classical RAIM methods as initially suggested by [3] for code-based single-point processing in aviation applications. This approach is based on a consistency check of the over-determined navigation solution and uses the following residual based test statistic:

$$\mathrm{RMS}(\mathbf{f}) \approx \sqrt{\frac{\sum_{j=1}^{m} f^{j^2}}{m-1}} \qquad (35)$$

$$f^j = {}^{n-1,n}D\tilde{\Phi}^j - {}^{n-1,n}D\hat{\Phi}^j$$

For sampling rates of 1 Hz or higher, $\mathrm{RMS}(\mathbf{f})$ is very low as all errors other than the ones caused by cycle slips or other outliers virtually vanish. This causes distinct spikes in the test statistic in the presence of outliers allowing for their detection and exclusion. Note that this approach requires the incremental solution which therefore has to be calculated even when applying the over-all solution strategy. An elaborate explanation of the RAIM method in time-differential processing is beyond the scope of this tutorial. The interested reader is referred to [11].

3.3 External correction data

Also non-outlying, healthy measurements are afflicted by errors $D\chi_{\text{total}}$. When working with the present approach, these errors are growing with increasing processing time spans. For attenuating the error drift different measures are taken when implementing the navigation equations: Tropospheric signal delays are compensated for by the UNB3 model given in [4]. Ionospheric propagation delays (advances when working with phase observations) are accounted for by a thin layer model as indicated in the standard literature, e.g. [9]. Here, the total electron count (TEC) is computed from ionospheric correction maps provided free of charge by the Crustal Dynamics Data Information System in the IONEX format (www.cddis.gsfc.nasa.gov). Ephemeris error reduction is realized using final ephemeris products published online by the International GNSS Service (IGS, http://igscb.jpl.nasa.gov). Attenuating the range error resulting from the satellite clock frequency offset, which integrates to the satellite clock error, is

achieved by the use of 30 s sampled clock correction data published by IGS. As the clock error is growing faster than the ephemeris error, these corrections are particularly important when working with time differences. More details about the effect of the described correction models on the time difference solution is given by [15]. With Eq. (29) one can see that the error ${}^{bi}\nabla\chi_{\text{geo}}$ stemming from a bias in the base solution becomes maximum if $\Delta\xi_b$ is collinear with $\dot{\mathbf{e}}_i$. According to [17] $\|\dot{\mathbf{e}}_i\|$ does not exceed 0.00019 /s. For a processing interval of 200 s and a base position bias of 4 m the resulting range error would be 15 cm in this worst case scenario. Hence it is important to apply the range corrections used for time differential processing to attenuate error drift also when calculating the base position via code based single point processing for absolute error limitation.

4.0 PRACTICAL VALIDATION

4.1 Static Experiment

The results of a static experiment are discussed in order to demonstrate the precision achievable by the time difference approach under good conditions. Moreover, the effect of the geometric error stemming from an offset in the initial base position is analyzed. The test was performed on June 19th, 2006 on a sports field in the north of Munich with scattered buildings nearby (48°16'52.3'' N; 11°40'30.2'' E). The low cost receiver used is a u-Blox TIM-LP single frequency module integrated in an evaluation kit provided by the manufacturer. Zero baseline tests show the standard deviation of the phase measurements of the receiver to be as low as 0.87 mm [12]. For processing, ionospheric correction maps (igsg0190.06i), precise ephemeris (COD13584.EPH) and clock corrections (COD13584.CLK) are used. A time interval of 5 min is processed, which is significantly longer than the typical intervals to be analyzed for flight measurements.

The bold red line of the upper plot of Figure 6 shows the error drift of the over-all solution during this time interval, i.e. the offset of the static relative solution from zero. Good PDOP vales of about 2.1, see lower plot, limit the error to below 3 dm. Besides the error, the estimate of the error is illustrated by the upper plot of Figure 6: The lowest, dashed green line is the root mean square of the phase range residuals, the light blue line right above is the estimate of the standard deviation of the measurements, compare Eq. (32). Scaling with PDOP yields the 3D position error estimate as given by Eq. (34). Considering the simplifications made for calculating this estimate indicated by the bold, dotted, grey line, it matches the actual error well. However, one has to be aware that the quality of the error estimate depends on the number of used satellites and will be meaningless for the case of only four used satellites. The impact of a bias in the base position was discussed theoretically by Eqs. (25) through (29) and illustrated by Figure 4. This effect is validated by adding an offset vector $\delta\mathbf{x}_b$ with random direction but defined length to the best estimate of the initial solution as used above. The results are shown by Figure 7:

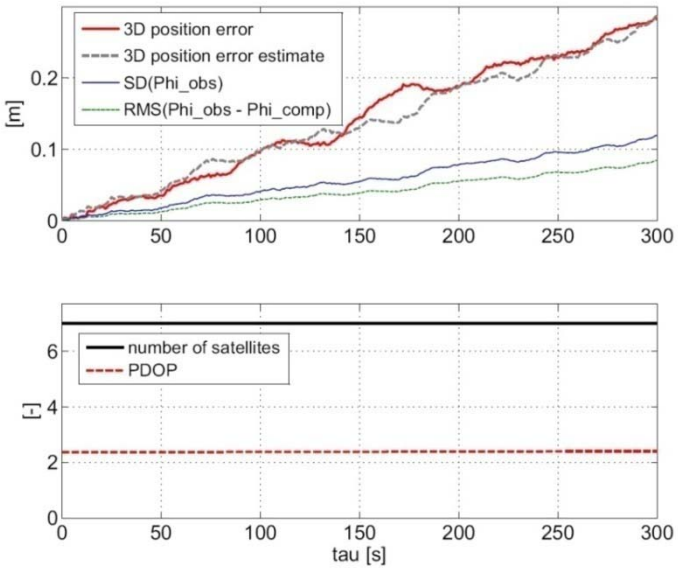

Figure 6: Static test: 3D error with quality assessment.

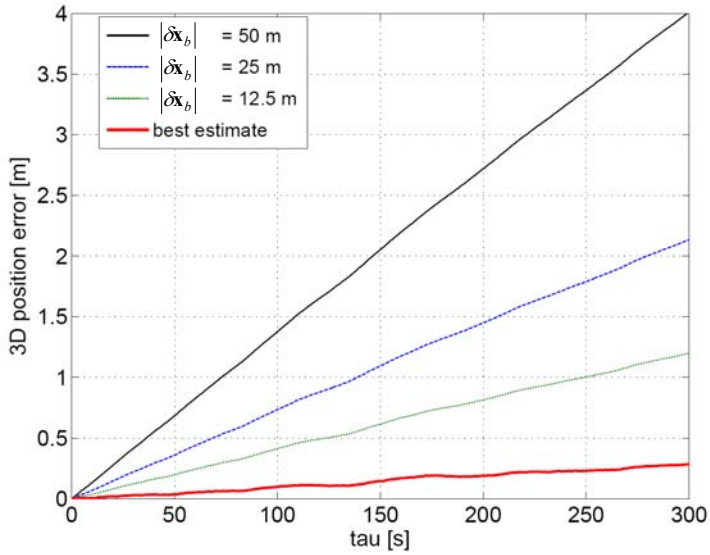

Figure 7. Static test: impact of a bias in the base position on relative precision

One can clearly see a (linear) relationship between the offset in the base position and the growing drift in the time difference solution. These results coincide well with Eq. (29) and underline the need for a good estimate of the base position and time solution. However, the results of this static test also show that the precision of the time difference solution obtained when applying all mentioned corrections stays in the low decimeter (or even centimeter) range depending on the time spans to be analyzed.

4.2 Dynamic Flight Experiment

HARDWARE. The test was performed using the miniaturized GPS data-logger depicted in Figure 8.

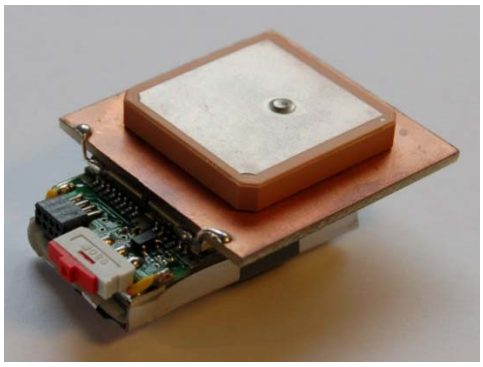

Figure 8: Miniaturized GPS datalogger with 25×25 mm^2 patch antenna attached

This receiver features the u-Blox module LEA-4T capable to provide raw GPS data. Signals are acquired by a 25 × 25 ×4 mm^3 passive patch antenna placed on 35 × 35 mm^2 ground plate. In addition to the onboard PT solution available with up to 4 Hz, non processed raw data with a sampling rate of up to 10 Hz can be logged within the 8 MB internal flash memory (approximately 40 min of recording at 10 Hz). The quality of the raw data is expected to be comparable to those of the TIM-LP receiver used for the static test. The form factor of the logger is as small as 44×21×4 mm^3 at a weight of 4.25 g only without battery. Adding the patch antenna (14.15 g) and a 320 mAh 3.7 V lithium-polymeric battery (7.1 g) increased weight of the construction up to 25.5 g. The power consumption is approximately 40 mA. The available logging memory is extended by connecting an external serial datalogger featuring a 2 GB SD memory card. The volume of the serial data logger is 50 × 36 ×5 mm^3, its weight is 6 g and its power consumption is 6.7 mA. 2 GB of memory is sufficient to store 10 Hz raw GPS data during 8 days approximately.

FLIGHT TEST WITH ACROBATIC PLANE. The flight was performed by the acrobatic plane Mü30 "Schlacro" developed and built by the academic aviation association AKAFLIEG of TU München. The receiver was mounted on the outer left wing tip of the aircraft, as illustrated by Figure 9.

**Figure 9: Mü30 flight test: Aircraft Mü30 "Schlacro"
with GPS logger mounted on left wing tip**

The 10 Hz phase data collected during a S-sequence maneuver flown close to the airfield Fürstenfeldbruck, Germany, on August 15th, 2008, is analyzed. The 2D trajectory and the vertical profile of the maneuver are given by Figure 10.

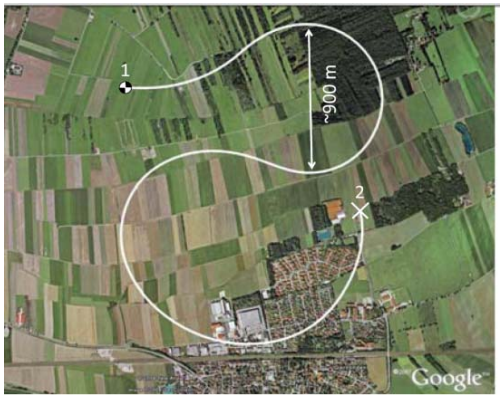

(a) 2D trajectory. (1) Start of precise relative processing; (2) end of precise relative processing

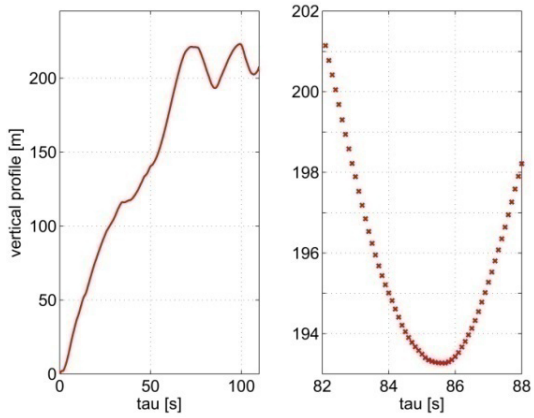

(b) Vertical profile relative to the starting point (1) of the maneuver. Total time history (to the left) and zoomed section

Figure 10: Mü30 flight test: flight trajectory during S-sequence maneuver.

When processing, precise ephemeris, high rate clock solutions and ionospheric correction maps are used. The quality of the collected phase measurements is good, the root mean square of the C/N0 values yields 48.1 dBHz. As a consequence, the residual level and the estimate of the measurement standard deviation dropping out from the least squares solver are very low, see light green and blue lines in the upper plot of Figure 11.

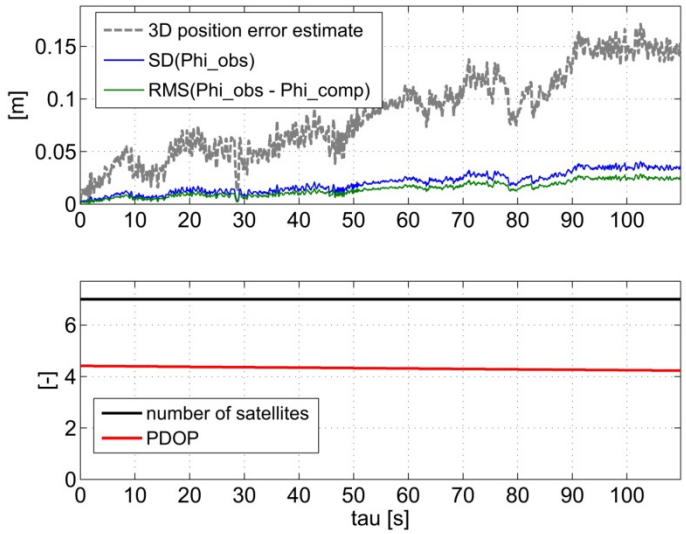

Figure 11: Mü30 flight test: quality analysis of the time difference solution

The geometry of the available satellite subset results in PDOP values of up to 4.4, lower plot of the figure. These values are combined to the 3D error estimate, Eq. (34), indicated by the bold grey line of the upper plot of Figure 11 The precision is estimated to be better than 17 cm. For validation purposes, a second receiver (u-Blox TIM-LP) was mounted close to the airfield serving as a base station for RTK processing and static initialization was provided. The fixed solution is computed in a differential (RTK) mode using

the data of the base receiver. The double-differenced phase and code data of both receivers are processed using inhouse Kalman filter software of the Department of Earth Observation & Space Systems of Delft University of Technology [14]. It is well worth to note that aside from serving as a validation of the time difference method, the RTK solution also demonstrates successful ambiguity resolution when processing data of truly low cost receivers collected in highly dynamic applications. The deviation of the obtained results from the time difference solution is shown by Figure 12. The relative error components in local tangent coordinates do not exhibit a special trend to the height direction and the absolute value of the 3D relative offset stays below 13 cm. This result confirms the high precision achievable by time differences.

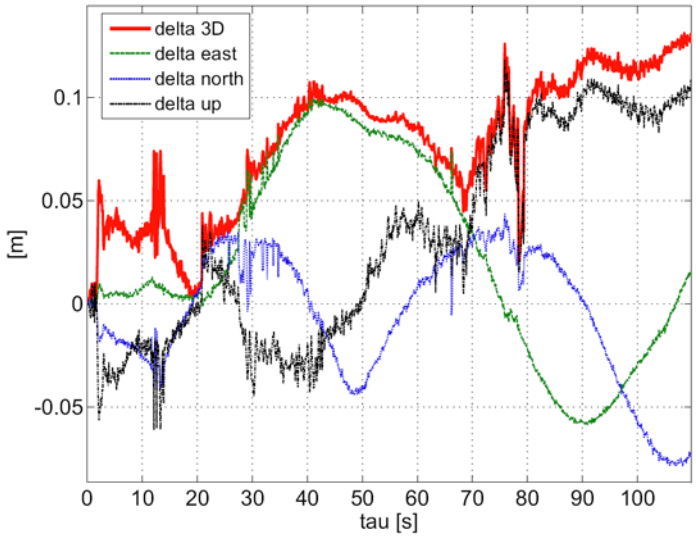

Figure 12: Mü30 flight test: comparison of the time difference method with a RTK solution generated by DEOS of TU Delft [14]

5.0 IN FLIGHT MEASUREMENTS OF DYNAMIC SOARING OF ALBATROSSES

The Wandering Albatross lives predominantly at very remote places of the southern hemisphere. As a consequence, the realization of our measurement campaign during the arctic summer 2008/09 at Kerguelen Archipelago (Figure 13 (a)) was only possible in cooperation with our partners from the Centre d'Ecologie Fonctionnelle et Evolutive of the French Centre National de la Recherche Scientifique contributing the indispensable ornithological and logistical expertise. As recovering the receivers after application on the birds was required, measuring took place during the breeding period, when the birds take turns leaving their nest for up to 30 day lasting foraging trips over open waters.

(a) Kerguelen Archipelago

(b) Wandering Albatross equipped with GPS receiver

Figure 13: GPS measurement campaign during the arctic summer 2008/09

The birds where equipped with hardware comparable to the receiver presented in section 0. Power was supplied by three lithium-thionyl-Chloride AA-type primary cells. The mass of the complete logging unit did not exceed 100 g. Some receivers additionally featured 3 axis MEMS accelerometers. Mounting on the bird was realized using adhesive tape, see Figure 13(b). 16 flights / flight sections where successfully recorded, two of them are shown in Figure 14 (a) and (b).

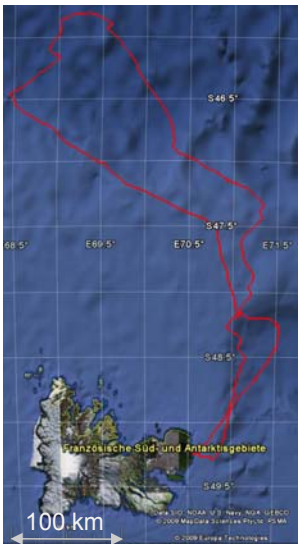

(a) 3 day foraging trip

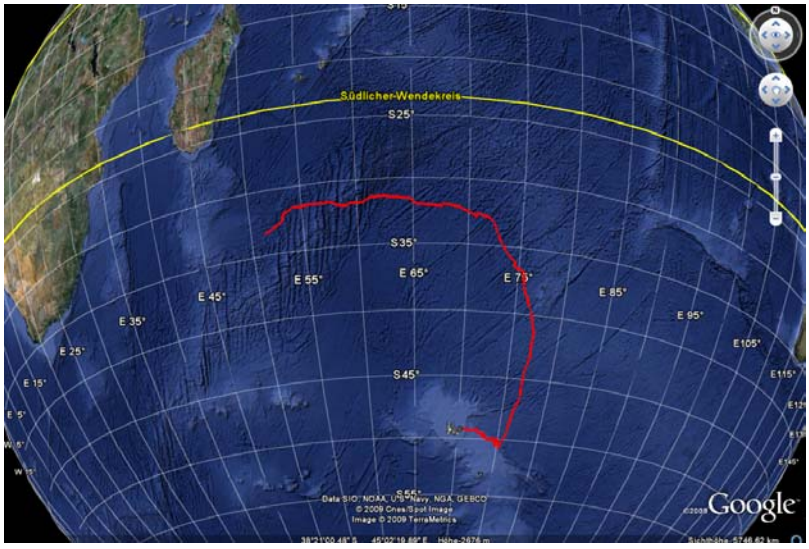

(b) First 6 days of a 30 day trip

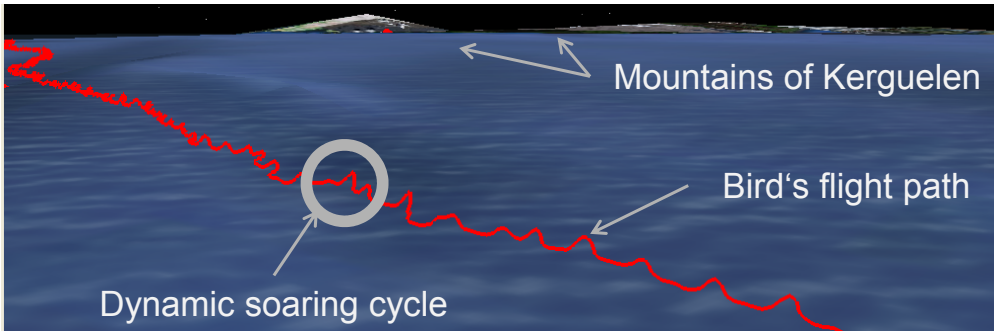

(c) 3D view of the bird’s trajectory with dynamic soaring cycles

Figure 14: GPS tracks of foraging Wandering Albatrosses

5.1 Analysis of an Exemplary Dynamic Soaring Cycle

For understanding the dynamic soaring technique, the global trajectories are of secondary interest only but individual flight cycles as shown in Figure 14 (c) are to be analyzed precisely using the time differential technique. The processing results of an exemplary cycle are discussed in the below.

Figure 15 shows a randomly chosen flight cycle. In the left-hand side plot, the vertical component is scaled by a factor of three for improving the perspective perception. The time history of the vertical component of the 16 second lasting maneuver already gives an impression of the precision of the time-differential solution, Figure 15 (b). The solution was calculated applying the accumulation strategy; 5 to 9 satellites where available yielding PDOP values ranging from 1.8 to 5.5. The error drift is estimated to reach up to 0.9 dm – an estimate which is probably overly pessimistic, as mentioned below.

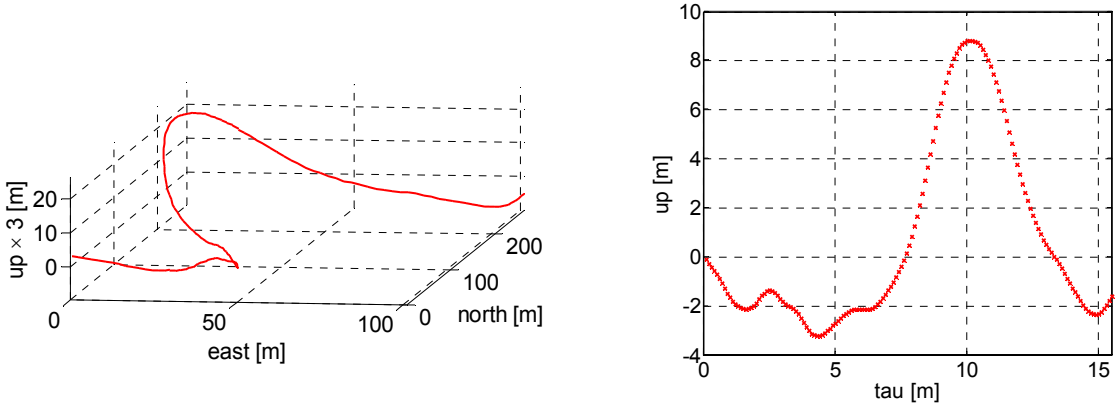

(a) 3D trajectory of an individual dynamic soaring cycle

(b) Time history of the vertical component

Figure 15: Dynamic soaring cycle processed using the time-differential technique

For further analysis the position fixes are transformed to an analytical form using cubic smoothing splines as a first approach. Such interpolation is shown for the vertical component by Figure 16. Here the smoothing parameter is chosen in a way that the spline residuals (bottom plot) are of the same order of magnitude than the 3D estimate of the noise component calculated according to Eq. (34) using inter-epoch residuals, center plot. Staying below 2 cm, the residual level is very low considering the high dynamics of the maneuver.

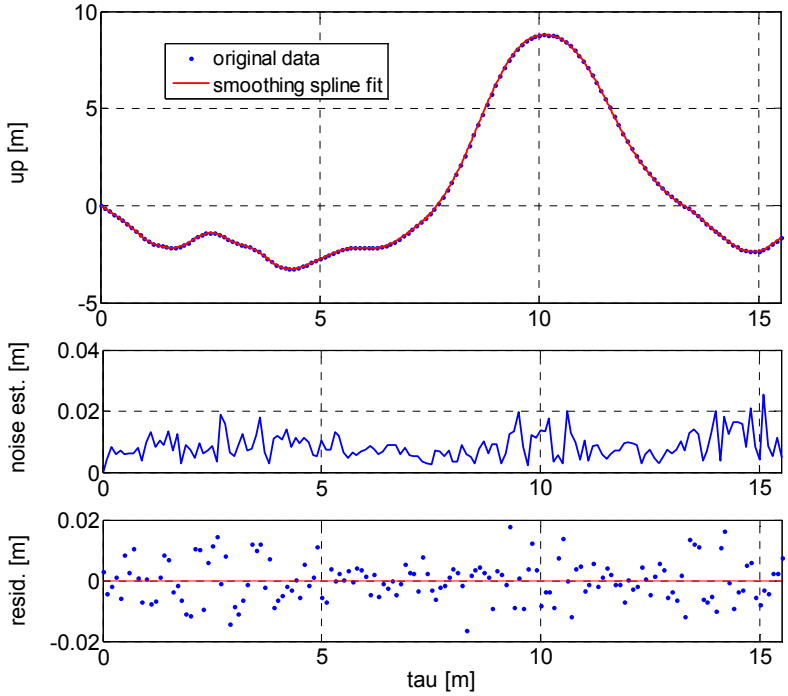

Figure 16: Interpolation and smoothing

The fitted position solution can now be used for velocity calculation – the blue line of the upper plot of Figure 17 illustrates the speed relative to the ground resulting from analytical derivation. The red dots of

the same plot are obtained by directly differentiating the position data (using MATLAB's diff command) without precedent smoothing. (Note that both solutions are significantly smoother than the solution obtained using the recorded Doppler measurements for single point processing, illustrated by the black circles). The lower plot shows the corresponding absolute acceleration: again the red dots are the result of MATLAB's diff command applied twice to the position data whereas the blue line is the second derivative of the analytical fitting results. The green line is the absolute acceleration as measured by the 3D MEMS accelerometer, also available with 10 Hz. Contrarily to the acceleration derived from the GPS position, this value comprises the gravity vector. The green and the blue line are not parallel due to the tilting of the accelerometer with respect to the east-north-up coordinate system. For the time being, the accelerometer results are only shown here as a coarse consistency check.

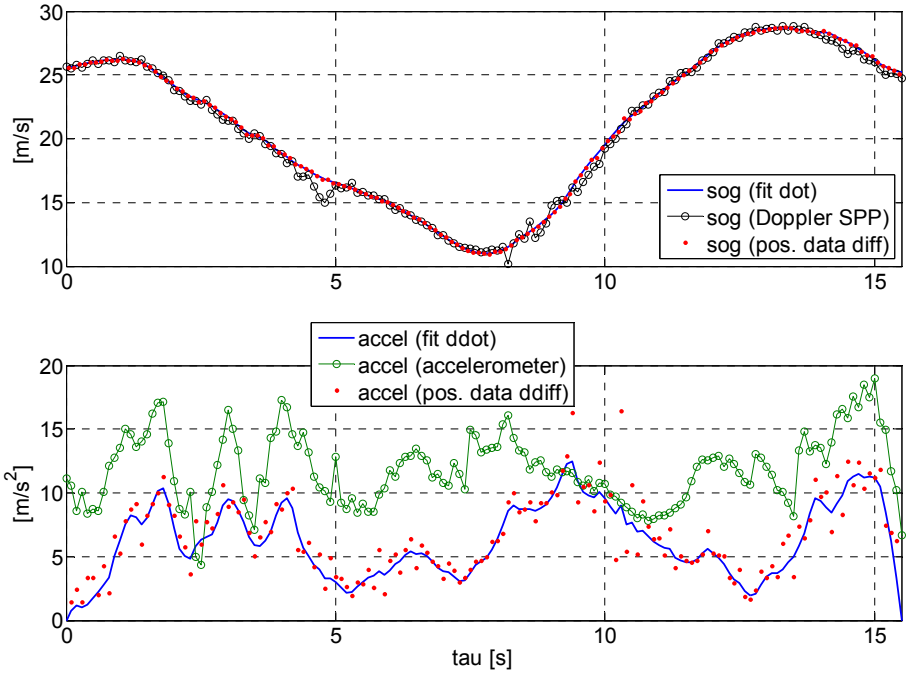

Figure 17: Dynamic soaring cycle processed using the time-differential technique

5.2 Outlook

This exemplary analysis aims to demonstrate the potential of the time-difference method applied to data gathered by miniaturized GPS receivers under rather difficult field conditions. Future work comprises aspects such as the development of more sophisticated interpolation methods, the recalibration and analysis of the used MEMS accelerometers (little is known about the quality of theses sensors by now) and of course the pursuit of the flight mechanical evaluation of the measured data.

6.0 CONCLUSIONS

Carrier phase time differences are used in a diversity of applications and recently also gain importance in safety critical applications such as receiver autonomous integrity monitoring for aviation applications. A method to utilize the fact of canceling ambiguities when forming time-differences as a standalone possibility to precisely process kinematic measurements over time spans of several minutes has been presented within this paper.

The navigation equations underlying this approach were derived and theoretical aspects of various error sources were reflected including an estimation of their impact on the final base vector precision. Further a short introduction to integrity monitoring and the outline of two different solution strategies for trajectory measurement was given.

The practical validation of static data gathered under favorable conditions confirmed that the temporal correlation of the remaining range errors is high. This allowed for processing time spans of up to 5 min with relative aberrations below 30 cm. Moreover, the test showed that the derived error estimate principally is a suitable means to assess the quality of the navigation solution. The impact of position biases of the base epoch was also demonstrated with the static data. Such offsets cause an additional "geometric" range error which can significantly distort the baseline. Applying the correction data used to attenuate the error drift also when calculating the initial position via code based single point processing is a suitable means to overcome this problem. Dynamic flight test results performed with a completely self-contained, miniaturized GPS logging device featuring a massmarket L1 single frequency GPS module were presented. Comparison with a fixed ambiguity RTK solution demonstrated that decimeter precision can be achieved even under very dynamic conditions.

The development of the time-difference method and the according hardware was triggered by the objective to measure the dynamic soaring of Albatrosses using GPS. This project was successfully realized during winter 2008/09. First results from this measurement campaign have been presented in this paper. The raw-data evaluation based on the time-difference method was demonstrated under navigational aspects and the subsequent data treatment yielding speed and even acceleration was shown.

The time-difference method is both unconventional and easy to apply in the field: For a user who is well aware of the pitfalls of raw phase data processing, neither a second, nearby base station along with (static) initialization procedures nor high quality receiver technology is required to achieve a truly phase based, stand-alone navigation solution precise to the low decimeter range. These advantages propose the application of the present approach not only for the unconventional task of the flight mechanical investigation of birds but for a wide panoply of other technical applications. One might think of measuring take-off or landing distances of aircraft during the certifications process or the quality assessment of trajectories autonomously flown by UAVs.

ACKNOWLEDGEMENTS

The authors would like to acknowledge Oliver Montenbruck, DLR, who strongly supported the development of the processing approach presented in this paper. Furthermore we would like to acknowledge AKAFLIEG of TU München for realizing the flight experiments with the aircraft Mü30 "Schlacro" and the Department of Earth Observation and Space Systems of TU Delft, namely Dennis Odijk, for providing the RTK reference solution. Special thanks shall be directed to Anna Nesterova and Francesco Bonadonna from Centre d'Ecologie Fonctionnelle et Evolutive, CNRS, Montpellier. Without their support the Albatross measurement campaign would not have been possible.

REFERENCES

[1] Balard, N., R. Santerre, M. Cocard and S. Bourgon (2006). "Single GPS receiver time-relative positioning with loop misclosure corrections." *GPS Solutions*, Vol. 10, No. 1, pp. 56-62.

[2] Becker, M., U. Bestmann, A. Sasse, M. Steen and P. Hecker (2007). "In Flight Estimation of Gyro and Accelerometer Scale Factors for Tactical and MEMS IMUs." *Proc.of ION 20th International Techical Meeting of the Satellite Devision*, Fort Worth, TX, 25-28 September 2007, pp. 2056-2065.

[3] Brown, R.G. and C.Y. Chin (1997). "GPS RAIM: Calculation of Threshold and Protection Radius Using Chi-Square Methods – A Geometric Approach." Global Positioning System: Inst. of Navigation, vol. V, 1997

[4] Collins, P.C., R. Langley and J. LaMance (1996). "Limiting Factors in Tropospheric Propagation Delay Error Modelling for GPS Airborne Navigation." *Proc. of ION 52nd Annual Meeting*, Cambridge, MA, 1996.

[5] Farrell, J.L. (2001). "Carrier phase processing without integers. *Proc. of ION 57th annual meeting/CIGTF 20th biennial guidance test symposium,* Albuquerque, NM, 11-13 June 2001, pp. 423-428.

[6] ESA – European Space Agency (2005). "EGNOS Fact Sheet 14 – SBAS – Interoperability Explained – Delivering a Global Service", available online in August 2009 at http://www.egnos-pro.esa.int/Publications/fact.html

[7] Gao, Y. (2006). "What is precise point positioning (PPP), and what are its requirements, advantages and challenges?" *InsideGNSS,* Vol. 1, No. 8, pp. 16-18.

[8] van Graas, F and S.-W. Lee (1995). "High-accuracy differential positioning for satellite-based systems without using code-phase measurements." *Journal of the Institute of Navigation*, Vol. 42, No. 4, pp. 605-618.

[9] Hofmann-Wellenhof, B., H. Lichtenegger and J. Collins (2001). "Global Positioning Systems, Theory and Practice", 5th edition, Springer, Wien, New York.

[10] Kim, D. and R. Langley (2002). "Instantaneous real-time cycle-slip correction for quality control of GPS carrierphase measurements*." Journal of the Institute of Navigation*, Vol. 49, No. 4, pp. 205-222.

[11] M. Kirkko-Jaakkola, J. Traugott, D. Odijk, J. Collin, G. Sachs and F. Holzapfel (2009). "A RAIM approach to GNSS outlier and cycle slip detection using L1 carrier phase time-differences." Proceedings of the IEEE Workshop on Signal Processing Systems, Tampere, Finland, October 2009.

[12] Odijk, D., J. Traugott, G. Sachs, O. Montenbruck and C.C.J.M. Tiberius (2007). "Two Approaches to Precise Kinematic GPS Positioning with miniaturized L1 Receivers." *Proc. of ION 20th International Techical Meeting of the Satellite Division*, Fort Worth, TX, 25-28 September 2007, pp. 827-838.

[13] Sachs, G. (2005). "Minimum Shear Wind Strength Required for Dynamic Soaring of Albatrosses." *Ibis*, Vol. 147, pp. 1-10, 2005.

[14] Teunissen, P.J.G. (1994). „A New Method for Carrier Phase Ambiguity Estimation." *Proc. of IEEE PLANS*, Las Vegas, NV, 11-12 April 1994, pp. 862-873.

[15] Traugott, J., D. Odijk, O. Montenbruck and C.C.J.M. Tiberius (2008). "Making a Difference with GPS." *GPS World*, Vol. 19, No. 5, pp. 48-57.

[16] Traugott, J. (2009). "Measuring the dynamic soaring of Albatrosses by time-differential processing of phase measurements from miniaturized L1 GPS receivers." *Presentation at the Colloquium of Satellite Navigation of Technische Universtitä München*, June 2009. http://www.nav.ei.tum.de → Colloquium → Summer Term 2009

[17] Ulmer, K., P. Hwang, B. Disselkoen and M.Wagner (1995). „Accurate azimuth from a single PLGR+GLS DoD GPS receiver using time relative positioning." *Proc. of ION GPS-95*, Palm Springs, CA, 12-15 September 1995, pp. 1733-1741.

[18] Vyssotski, A.L., A.N. Serkov, P.M. Itskov, G. Dell'Omo, A.V. Latanov, D.P. Wolfer and H.-P. Lipp (2006). "Miniature Neurologgers for Flying Pigeons: Multichannel EEG and Action and Field Potentials in Combination with GPS Recording." *Journal of Neurophysiology*, Vol. 95, pp. 1263-1273.

[19] Walter, T., J. Blanch, P. Enge, B. Pervan and L. Gratton (2008). "Shaping Aviation Integrity - Two RAIMs for Safety." *GPS World,* Vol. 19, No. 4, pp. 42-49.

[20] Wendel, J., T. Olbert and G.F. Trommer (2003). "Enhancement of a tightly coupled GPS/INS system for high precision attitude determination of land vehicles." *Proc.of ION 57th annual meeting/CIGTF 22nd guidance testsymposium,* Albuquerque, NM, 23-25 June 2003, pp.200-208.

[21] Weimerskirch, H., T. Guionnet, J. Martin, S.A. Shaffer and D.P. Costa (2000). "Fast and Fuel Efficient? Optimal Use of Wind by Flying Albatrosses." *Proc. R. Soc. Lond.* B 267, pp. 1869-1874.